Electron paramagnetic resonance and photoluminescence study of Er-impurity complexes in Si

J. D. Carey,* R. C. Barklie, and J. F. Donegan
Department of Physics, Trinity College, Dublin, Ireland

F. Priolo
INFM and Dipartimento di Fisica, Università di Catania, Corso Italia 57, I 95129 Catania, Italy

G. Franzò and S. Coffa
CNR-IMETEM, Stradale Primosole 50, I 95121 Catania, Italy

(Received 27 April 1998; revised manuscript received 6 August 1998)

Electron paramagnetic resonance (EPR) and photoluminescence (PL) spectroscopy have been used to examine the structure and optical properties of erbium-impurity complexes formed in float-zone Si by multiple-energy implants at 77 K of Er together with either O or F. After implantation a 2-μm-thick amorphous layer was formed containing an almost uniform concentration of Er (10^{19}/cm^3)and O (3×10^{19}/cm^3 or 10^{20}/cm^3) or F (10^{20}/cm^3). Samples were annealed in nitrogen at 450 °C for 30 min (treatment *A*), treatment *A*+620 °C for 3 h (treatment *B*), treatment *B*+900 °C for 30 s (treatment *C*) or treatment *B*+900 °C for 30 min (treatment *D*). Samples coimplanted to have 3×10^{19} O/cm^3 and subject to treatment *C* show a broad line anisotropic EPR spectrum. These samples have the most intense low-temperature PL spectrum containing several sharp peaks attributed to Er^{3+} in sites with predominantly cubic T_d symmetry. Increasing the O concentration to 10^{20}/cm^3 produces sharp line EPR spectra the strongest of which are attributed to two Er^{3+} centers having monoclinic C_{1h} and trigonal symmetry. The principal g values and tilt angle for the monoclinic centers are $g_1=0.80$, $g_2=5.45$, $g_3=12.60$, $\tau=57.3°$, $g_\parallel=0.69$, and $g_\perp=3.24$ for the trigonal centers. The low-temperature PL spectrum from this sample showed additional sharp lines but the total intensity is reduced when compared to the sample with 3×10^{19} O/cm^3. For the sample containing 10^{20} O/cm^3 at least four distinct centers are observed by EPR after treatment *B* but after treatment *D* no EPR spectrum is observed. The PL spectra are also observed to change depending on the specific anneal treatment but even after treatment *D*, Er-related PL is still observed. Samples containing 10^{20} F/cm^3 and annealed with either treatment *B* or *C* produced an EPR spectrum attributed to Er^{3+}in a site of monoclinic C_{1h} symmetry with $g_1=1.36$, $g_2=9.65$, $g_3=7.91$, and $\tau=79.1°$.Tentative models for the structures of Er-impurity complexes are presented and the relationship between the EPR-active and PL-active centers is discussed. [S0163-1829(99)04503-8]

I. INTRODUCTION

Semiconductors doped with rare-earth ions are the subject of a considerable amount of research due to their applications in optoelectronics.[1–16] The *4f* electrons are shielded from the full effects of the host crystal field and this results in the intra-*4f* shell optical transitions being both sharp and nearly independent of the host material. Furthermore, due to the close proximity of the *4f* electrons to the nucleus, these electrons experience a strong spin-orbit interaction. Erbium doped silicon has attracted particular attention because the $^4I_{13/2}$ to $^4I_{15/2}$ transition in Er^{3+}occurs at the technologically important wavelength of 1.54 μm. This wavelength matches the minimum in the absorption of light in silica-based optical fibers and is thus important in optical fiber communication. When Er ions are incorporated into Si, this transition can be excited both optically[4] and electrically.[5] Indeed, Er doping of Si is one of the most successful ways in obtaining light emission from this semiconductor,[1,2] thus circumventing the intrinsic inability of Si to provide efficient light emission. One of the principal problems in the development of Er-doped Si has been the strong quenching behavior of both the photoluminescence (PL) and electroluminescence (EL) on going from 77 K to room temperature.[3,4] It had been observed that over this temperature range the PL intensity decreased by over three orders of magnitude. However, in the presence of suitable concentrations of impurities such as O or F it has been shown that the PL intensity decreased only by a factor of 30.[6] This has led to the observation of room-temperature EL from Er-doped Si *p-n* diodes codoped with O or F.[5,7] In addition to reducing the quenching of the PL, the presence of the impurities can increase the net solubility of Er in Si. The solid solubility[8] of Er in Si is low ($\sim2\times10^{16}$/cm^3) and to increase it nonequilibrium techniques such as molecular-beam epitaxy,[9,10] chemical vapor deposition,[11] or ion implantation[6,12] must be employed. At concentrations above the solubility limit, precipitation of Er into Er silicide will occur. Coimplantation with either O or F has been shown to help in suppressing precipitation and Er concentrations as high as of 1×10^{19}/cm^3 have been incorporated in a good-quality Si single crystal by ion implantation.[6,13] These beneficial effects have been attributed to modifications in the local environment of the Er atom through the formation of Er-impurity complexes.[14–16] It is therefore of great interest to determine the structure of these complexes. Some information has already been obtained from extended x-ray-absorption fine-structure (EXAFS) measurements, which showed that Er is surrounded by a cage of 4–6 O atoms.[15,16]

Electron paramagnetic resonance (EPR) is one of the most powerful experimental techniques used to examine defects and complexes in semiconductors.[17] Furthermore, EPR is able to distinguish between the two common Er valence states, Er^{2+} and Er^{3+}. Er^{2+}has 12 *4f* electrons and is thus a non-Kramers ion whereas Er^{3+}, having an odd number of electrons, is a Kramers ion.[17] To date there has only been one report[18] of a weak EPR signal from Er-doped Czochralski (CZ) grown Si but this was only observed with above-band-gap illumination. It was concluded that this EPR signal was due to an ionized state of a defect with a 2+ charge ground state; no Er-related photoluminescence was observed from this defect. Recently, we have reported a preliminary EPR study on Er-doped Si and indeed we have shown the presence of Er^{3+} centers in Si.[19] In this paper we present the first detailed EPR study of Er complexes in Si implanted with Er together with either O or F. We show that the nature of the coimplanted ions as well as their concentrations and the postimplantation anneal treatments all affect the structure and/or the concentration of the Er complexes. The relationship between the EPR-active centers and the optically active centers is examined using high-resolution PL measurements.

II. EXPERIMENT

Samples of *n*-type FZ (100) wafers (resistivity ~220 Ω cm) were implanted with Er ions at 77 K using a 1.7-MV tandem accelerator and a sputter ion source with an Er oxide cathode. All the samples investigated were implanted with Er to a total fluence of $1\times10^{15}/cm^2$ with energies in the range 0.5–5 MeV to give an approximately uniform concentration of 1×10^{19} Er/cm^3 over most of the implanted region. One sample (Er1) was only implanted with Er. The other samples were coimplanted with O or F at different energies in the range 0.15–0.5 MeV to give approximately uniform impurity concentrations in the region where Er resides. One sample (O1) has an O concentration of approximately $3\times10^{19}/cm^3$ in the region between 0.3 and 1.8 μm below the surface resulting in a nearly constant 3:1 O:Er concentration ratio in most of the implanted region as measured by secondary ion mass spectrometry (SIMS). A third sample (O2) was implanted with O in order to have an almost constant O concentration of $1\times10^{20}/cm^3$ and a 10:1 O:Er concentration ratio in most of the implanted region. After implantation a continuous amorphous layer extends from the surface to a depth of over 2.0 μm as measured by transmission electron microscopy (TEM). Each sample was annealed at 450 °C for 30 min to smooth the amorphous-crystalline interface and most were then subsequently annealed for 3 h at 620 °C in order to induce the solid phase epitaxial (SPE) recrystallization of the amorphous layer. Finally thermal annealing under flowing N_2 for 30 s or 30 min at 900 °C was performed on some of the samples.

To examine the effects of different post-implantation treatments, three samples, in addition to O2, each with 1×10^{19} Er/cm^3 and 1×10^{20} O/cm^3 were annealed under different conditions. Sample O3 was just annealed at 450 °C for 30 min (treatment *A*), and sample O4 was annealed at 450 °C for 30 min followed by 620 °C for 3 h (treatment *B*). Sample O5 received treatment *B* but was then subject to a high-temperature annealing at 900 °C for 30 min (treatment *D*).

TABLE I. Sample labels, implanted impurity concentrations and annealing treatments for the samples investigated. Treatment *A*: Annealed at 450 °C for 30 min. Treatment *B*: Annealed at 450 °C for 30 min+620 °C for 3 h. Treatment *C*: Annealed at 450 °C for 30 min+620 °C for 3 h+900 °C for 30 s. Treatment *D*: Annealed at 450 °C for 30 min+620 °C for 3 h+900 °C for 30 min.

Sample label	Impurity concentrations	Annealing treatment
Er1	1×10^{19} Er/cm^3	*C*
O1	1×10^{19} Er/cm^3+3×10^{19} O/cm^3	*C*
O2	1×10^{19} Er/cm^3+1×10^{20} O/cm^3	*C*
O3	1×10^{19} Er/cm^3+1×10^{20} O/cm^3	*A*
O4	1×10^{19} Er/cm^3+1×10^{20} O/cm^3	*B*
O5	1×10^{19} Er/cm^3+1×10^{20} O/cm^3	*D*
F1	1×10^{19} Er/cm^3+1×10^{20} F/cm^3	*B*
F1	1×10^{19} Er/cm^3+1×10^{20} F/cm^3	*C*

Finally to examine the effects of different coimplanted impurity atoms, two samples were coimplanted with F at 77 K. The same ion energies and doses were used for F coimplantation as were used in the coimplantation of sample O2 and this resulted in an nearly constant 10:1 F:Er concentration ratio in most of the implanted region. To examine the effects of different annealing conditions, one sample, labeled F1, was subjected to thermal treatment *B* (450 °C for 30 min +620 °C for 3 h). The second sample, F2, was subjected to treatment *C* (450 °C for 30 min+620 °C for 3 h+900 °C for 30 s). Table I summarizes the impurity content and annealing conditions of the samples examined.

EPR measurements were performed in a modified Bruker EPR spectrometer with 100 kHz field modulation using a TE_{102} rectangular cavity. The microwave frequency was approximately 9.23 GHz and the samples were cooled to helium temperatures using an Oxford Instruments flow cryostat. The sample temperature was approximately 10 K and care was taken not to saturate the EPR spectra with microwave power. Each of the samples were cleaved such that a [100] direction was parallel to the vertical sample rotation axis. This allowed the orientational dependence of the EPR spectrum in the (110) plane to be measured. PL measurements were performed using the 488-nm line of an Ar^+ laser with a pump power of 200 mW. The pump beam was focused to a 1-mm-diam spot on the sample and mechanically chopped at a frequency of 55 Hz. The PL signal was collected by two lenses, analyzed with a monochromator and detected with a North Coast liquid-nitrogen-cooled Ge detector. Spectra were recorded using a lock-in amplifier with the chopper frequency as a reference. Low-temperature measurements were performed by using a closed-cycle liquid-He cooler system with the samples kept in vacuum.

III. EXPERIMENTAL RESULTS

A. Effects of oxygen codoping on the EPR spectra of Er-doped Si

The low-temperature EPR spectrum from sample Er1 (not shown) revealed only a broad isotropic resonance corresponding to a *g* value of 10.5. The peak-to-peak linewidth of this line was 23 mT and the line shape of this broad reso-

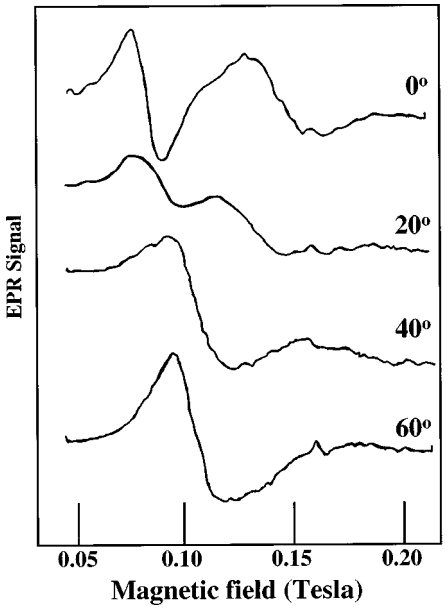

FIG. 1. Low-temperature EPR spectra from sample O1 (10^{19} Er/cm^3+3×10^{19} O/cm^3+450 °C for 30 min+620 °C for 3 h+900 °C for 30 s) at different orientations of the magnetic field in the (110) plane. The angle indicated is that between the magnetic-field direction and [001].

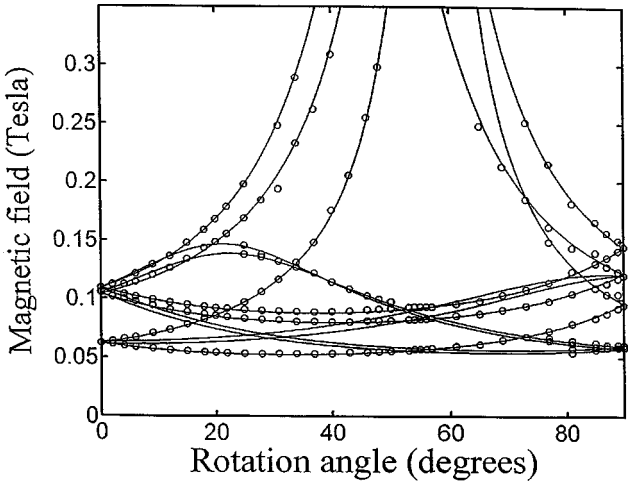

FIG. 3. Angular dependence of the observed resonances (open circles) from center OEr-1 in sample O2 (10^{19} Er/cm^3 +10^{20} O/cm^3+450 °C for 30 min+620 °C for 3 h+900 °C for 30 s) as the magnetic field is rotated in a plane near the (110) plane. Due to the slight misorientation of the sample, the magnetic field is not exactly in the (110) plane of the sample and this produces more lines than would be expected for C_{1h} symmetry. The fit (solid lines) is obtained from the principal g values and tilt angle given in the text.

nance did not change in a significant way as the magnetic field was rotated in the (110) plane of the sample. The EPR spectrum of sample O1, shown in Fig. 1, reveals the presence of two broad resonances which merge together as the magnetic field was rotated in the (110) plane through 60° from the [001] direction. No significant change in the spectrum occurred between 60° and 90°. In contrast to samples Er1 and O1, sample O2 has an EPR spectrum containing several sharp lines, as shown in Fig. 2, when the magnetic field is nearly parallel to [001]. Three distinct groupings of lines are evident: a series of sharp low-field lines in the range 0–0.15 T (lines 1–3), a broader line at approximately 0.25 T (line 4) and a single sharp isotropic line (not shown) with a g value of 2.004 57; the later is observed in all of the samples examined and we believe that this line originates from the underlying Si substrate. Lines 1–3 arise from centers (here labeled OEr-1) whose orientational dependence could be fitted, as shown in Fig. 3, to the effective spin Hamiltonian

$$H=\mu_B B\cdot g\cdot S \tag{1}$$

with $S=\frac{1}{2}$ and a g tensor exhibiting C_{1h} monoclinic symmetry. The principal g values are $g_1=0.80, g_2=5.45$, and $g_3=12.60$. The 2-axis lies in a $\langle 110\rangle$ direction and both the 1- and 3-axes lie in the plane perpendicular to it with the 1-axis tilted away by an angle τ from the [001] direction as shown in Fig. 4. For center OEr-1 the angle τ is 57.3°. These parameters were obtained by fitting the angular dependence of the spectrum as the magnetic field was rotated approximately with the (110) plane. The analysis shows that the rotation axis was not quite coincident with the $\langle 110\rangle$ direction with the result that the closest approach of the field direction to the [001] and [110] directions was 1.4° and 3.2°, respectively. The rotation angle is the angle through which the field is rotated and is defined to be zero at the closest approach to the [001] direction. It is this slight misalignment that leads to the splitting of lines 2 and 3 in Fig. 2 and the expected

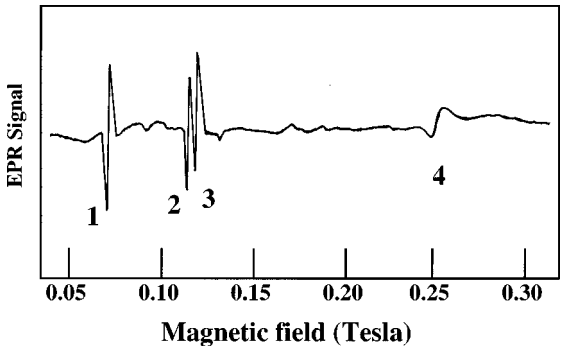

FIG. 2. Low-temperature EPR spectra from sample O2 (10^{19} Er/cm^3+10×10^{20} O/cm^3+450 °C for 30 min+620 °C for 3 h+900 °C for 30 s) for the magnetic field nearly parallel to the [001] direction. The microwave frequency was 9.23 GHz.

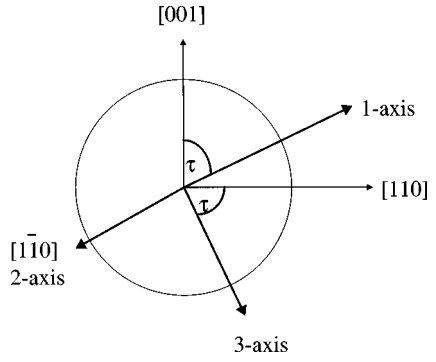

FIG. 4. The principal axes system for monoclinic C_{1h} symmetry. The 1-axis is tilted away from a $\langle 001\rangle$ direction by an angle τ. Both the 1- and 3-axes lie in the (110) plane and the 2-axis lies perpendicular to this plane.

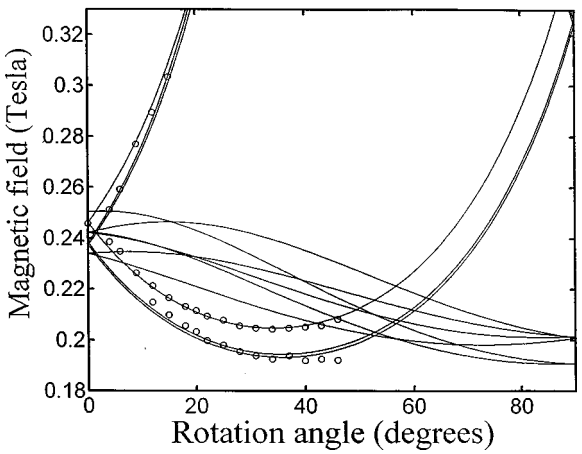

FIG. 5. Angular dependence of the observed low-field resonances (open circles) and fit for center OEr-2 in sample O2 (10^{19} Er/cm^3+10^{20} O/cm^3+450 °C for 30 min+620 °C for 3 h+900 °C for 30 s). The same misorientation parameters as used in center OEr-1 are used in the analysis of center OEr-2.

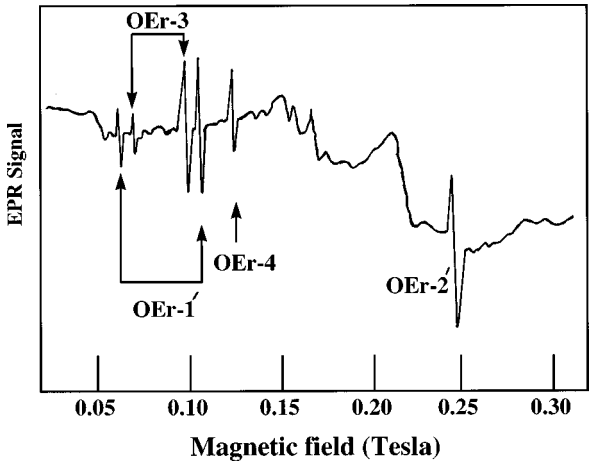

FIG. 6. Low-temperature EPR spectra from sample O4 (10^{19} Er/cm^3+10^{20} O/cm^3+450 °C for 30 min+620 °C for 3 h) for the magnetic field parallel to the [001] direction. The microwave frequency was 9.23 GHz. For convenience the lines associated with the centers OEr-1′, OEr-3, OEr-4, and OEr-2′ for this orientation are indicated on the spectrum.

presence of 12 lines in the angular dependence of the spectrum shown in Fig. 3 rather than the seven that would be expected for C_{1h} symmetry if the magnetic field was exactly in the (110) plane.[19]

Line 4 in Fig. 2 has a peak-to-peak linewidth of 7.7 mT but splits into several lines as the field direction is rotated away from [001]. Figure 5 shows the angular dependence of these lines as the magnetic field is rotated in approximately the (110) plane (the misorientation is the same as that described above). As the rotation angle was increased, the intensities of these lines diminished sharply and it was not possible to follow the lines beyond a rotation angle of about 45°. Using the available data it was possible to fit them by using the same monoclinic Hamiltonian as in Eq. (1). The principal g values obtained from the fitting are $g_1=0.45, g_2=3.46$, and $g_3=3.22$. The tilt angle τ is 55.9° and this center is labeled OEr-2. Since $g_2 \approx g_3$ and τ is close to 54.74° the center exhibits near trigonal symmetry. The fact that the line positions were only obtained for a limited angular range limits the reliability of the fit and the subsequent g values obtained for it. However, as presented in Sec. III B, we observe a more intense signal in another sample (O4), for which no misorientation occurred, which we believe is due to the same center and for which the full angular dependence was obtained to allow a more accurate determination of the g values. For none of the spectra, which for reasons given in the discussion we suggest are associated with Er^{3+} centers, were we able to detect the hyperfine lines associated with the 23% abundant Er^{167} isotope with $I=\frac{7}{2}$.[20]

B. Effects of different annealing treatments on the EPR spectra of the O codoped samples

The samples labeled O2, O3, O4, and O5 have the same impurity concentrations (10^{19} Er/cm^3+10^{20} O/cm^3) but have been subjected to different thermal annealing treatments. The results for sample O2 are given in the previous section. From sample O3 and sample O5 no Er-related EPR was observed, whereas from sample O4 many lines were observed most of which are associated with Er^{3+} complexes. Figure 6 shows the EPR spectrum from sample O4 obtained for the magnetic field parallel to the [001] direction. No misorientation of the sample in the magnetic field occurred in this case. Upon rotation of the magnetic field in the (110) plane a complicated orientational dependence was observed. The angular dependence of many of these lines could only be accounted for by assuming the presence of four different centers. Two of these centers OEr-1′ and OEr-3 exhibit monoclinic symmetry and the other two, OEr-2′ and OEr-4 exhibit trigonal symmetry. Table II lists the principal g value and tilt angles obtained from the fits to the angular dependence for each

TABLE II. Principal g values for the different centers observed in samples O2, O4, and F1.

Sample	Center	g_1	g_2	g_3	Average g value[a]	Tilt angle
O2	OEr-1	0.80	5.45	12.60	6.28	57.30°
O4	OEr-1′	0.80	5.45	12.55	6.27	56.90°
O4	OEr-3	1.09	5.05	12.78	6.31	48.30°
O4	OEr-4	2.00	6.23	6.23	4.82	54.74°
O2	OEr-2	0.45	3.46	3.22	2.38	55.90°
O4	OEr-2′	0.69	3.24	3.24	2.39	54.74°
F1	FEr-1	1.36	9.65	7.91	6.31	79.10°

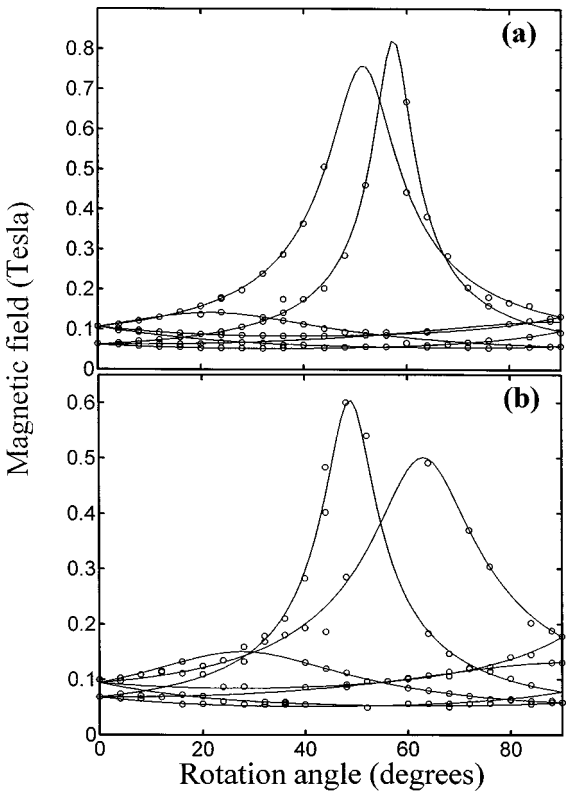

FIG. 7. Angular dependence of the observed low-field resonances (open circles) and fit (continuous line) for monoclinic centers: (a) center OEr-1′ and (b) center OEr-3 observed from sample O4 (10^{19} Er/cm^3+10^{20} O/cm^3+450 °C for 30 min+620 °C for 3 h). The same temperature is approximately 10 K and the microwave frequency is 9.23 GHz.

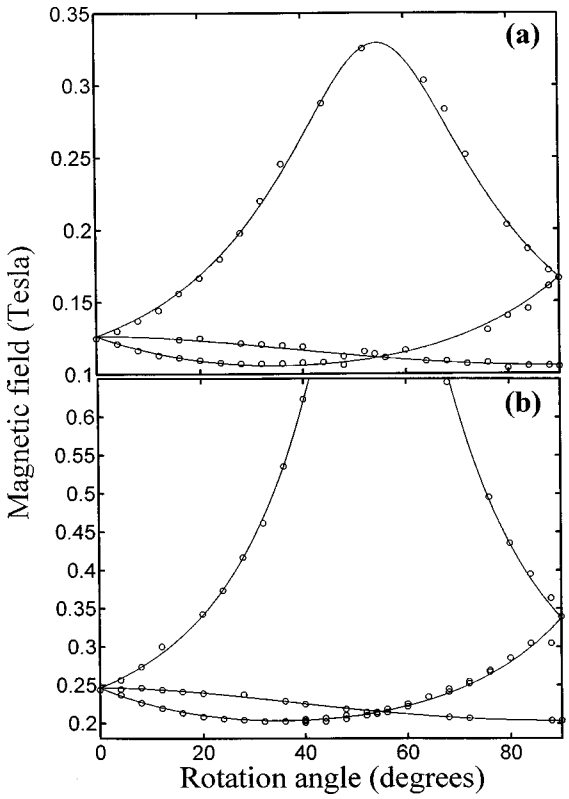

FIG. 8. Angular dependence of the observed low-field resonances (open circles) and fit (continuous line) for trigonal centers: (a) center OEr-4 and (b) center OEr-2′ observed from sample O4 (10^{19} Er/cm^3+10^{20} O/cm^3+450 °C for 30 min+620 °C for 3 h). The same temperature is approximately 10 K and the microwave frequency is 9.23 GHz.

center. Figure 7(a) and 7(b) show the fits obtained to the angular dependence for the monoclinic centers and Fig. 8(a) and 8(b) the fits to the data for the trigonal centers. The g values and tilt angle obtained from the fit to the data in Fig. 7(a) are the same, within the fitting error, as those obtained for center OEr-1. Consequently we believe that this center, labeled OEr-1′ is the same as center OEr-1 found in sample O2. Furthermore since the g values and tilt angle obtained from the fit to the data shown in Fig. 8(b) are similar to those obtained for center OEr-2, we believe that this center, here labeled OEr-2′, is the same as center OEr-2. Since the full angular dependence within the (110) plane was obtained for OEr-2′ it is likely that its parameters, given in Table II, are more reliable than for OEr-2.

A number of other unlabelled weaker lines, particularly around 160–170 mT, are seen in Fig. 6. It was not possible to perform a detailed angular dependence measurement on these lines as their intensity diminished upon rotation and these lines are subsequently masked by more intense lines the positions of which are changing as the orientation of the sample changes in the magnetic field; consequently we have not attempted to determine the principle g values of the centers associated with them.

C. Photoluminescence spectra of O-doped samples

Figure 9 shows the high-resolution (~10 Å) photoluminescence spectra from samples O1, O2, and O4 taken at 15 K. The PL spectrum from sample O1 reveals the presence of four dominant lines at wavelengths of 1.5376, 1.5559, 1.5748, and 1.5991 μm. The strongest of these lines is at 1.5376 μm and has a half-width at half-height of 9.2 cm^{-1}. The PL spectrum of sample O2 also contains these lines as well as extra lines. The half-width at half-height of the peak at 1.5376 μm from sample O2 is 11.9 cm^{-1}. The temperature dependence of the PL intensity from the two samples has also been studied.[13] Whilst the intensity of the 1.537-μm peak in sample O1 at 15 K is approximately a factor of 3 stronger compared to that of sample O2, at RT the corresponding signal is the same in the two samples. As can be seen from Fig. 9 the PL intensity of sample O2 is larger than that found from sample O4. Although both samples have the same impurity concentrations, sample O2 received an additional high-temperature anneal of 900 °C for 30 s (treatment *C*).

D. EPR and PL measurements of F coimplanted samples

Figure 10(a) shows the low temperature (~10 K) EPR spectrum of sample F1 (10^{19} Er/cm^3+10^{20} F/cm^3, thermal treatment *B*) with the magnetic field parallel to the [110] direction. Three lines are observed and peak-to-peak linewidths of the most intense lines are 1.2 mT (line 2) and 1.45 mT (line 3); the spectrum was unobservable above 17 K. The orientational dependence of the spectrum could be fitted, Fig. 10(b), to a single spin-$\frac{1}{2}$ monoclinic C_{1h} center, labeled

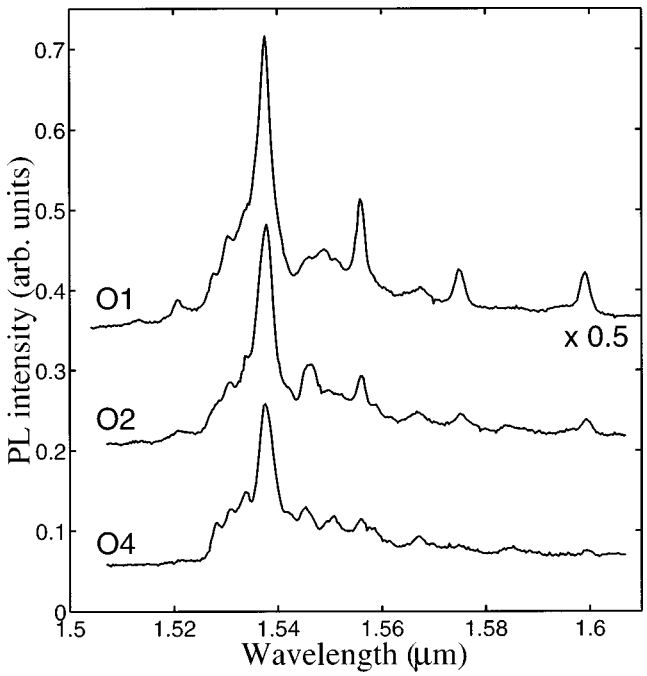

FIG. 9. Low-temperature photoluminescence spectra from sample O1 (10^{19} Er/cm^3+3×10^{19} O/cm^3+450 °C for 30 min +620 °C for 3 h+900 °C for 30 s), sample O2 (10^{19} Er/cm^3 +10^{20} O/cm^3+450 °C for 30 min+620 °C for 3 h+900 °C for 30 s), sample O4 (10^{19} Er/cm^3+10^{20} O/cm^3+450 °C for 30 min +620 °C for 3 h). The pump power was 200 mW.

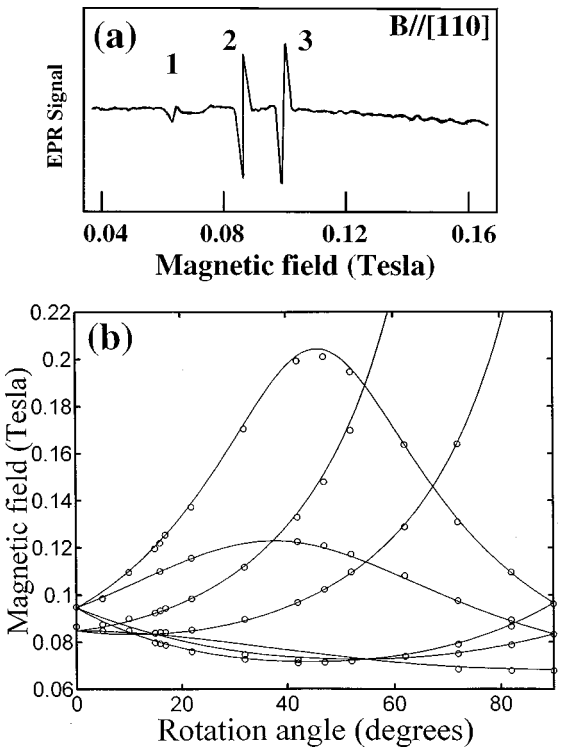

FIG. 10. (a) Low-temperature EPR spectrum from sample F1 (10^{19} Er/cm^3+10^{20} F/cm^3+450 °C for 30 min+620 °C for 3 h) with the magnetic field parallel to the [110] direction. (b) Angular dependence of the observed resonances (open circles) from sample F1 (10^{19} Er/cm^3+10^{20} F/cm^3+450 °C for 30 min+620 °C for 3 h) and fit (solid lines) attributed to a single Er^{3+} center with C_{1h} symmetry. This center is labeled FEr-1.

FEr-1, with principle g values $g_1=1.36, g_2=9.65$, and $g_3=7.91$ and a tilt angle of 79.1°. The fourth EPR line expected for C_{1h} symmetry for the magnetic field parallel to the [110] direction is beyond the magnetic-field range investigated. To investigate the thermal stability of the center FEr-1 sample F1 was annealed under flowing Ar for 15 min the intervals successively at 800, 840, and 870 °C. After each anneal the sample was cooled to 10 K and the spectrum recorded for the magnetic field parallel to the [110] direction. After annealing at 800 and 840 °C the intensities of lines 2 and 3 had both fallen to 65% and 40%, respectively, of their initial values. No EPR signal from center FEr-1 was detected after annealing at 870 °C. We also recorded the EPR spectra of another sample F2, which was codoped in the same way as F1 but which had received a 30 s anneal at 900 °C in addition to the anneals at 450 °C and 620 °C (treatment *C*). This sample gave the same spectrum as F1 but reduced in intensity by about a factor of 2. That the spectrum was seen at all despite the final anneal temperature exceeding 870 °C is undoubtedly due to the fact that the anneal at 900 °C was only for 30 s. The PL spectrum from sample F2 has been reported previously[13] and shows that Er-related luminescence is still observable though it is weaker and has a different shape than the corresponding luminescence from sample O2. This indicates that a different optically active Er center is present.

IV. DISCUSSION

Er^{3+} with eleven 4*f* electrons has a spin-orbit ground state of $J=\frac{15}{2}$ and is separated from the first excited state $^4I_{13/2}$ by ~6500 cm^{-1}.When the Er atom is incorporated into the Si host, the 16-fold degenerate free ion ground-state energy level is split into a number of Stark levels. The number and type of sublevels can be obtained from group theory and are given by the irreducible representation of the symmetry groups into which the J representation decomposes.[21] The decomposition of $J=\frac{15}{2}$, in T_d symmetry, can be shown to be[22]

$$D^{J=15/2}=\Gamma_6+\Gamma_7+3\Gamma_8. \tag{2}$$

The Γ_6 and Γ_7 are two-dimensional representations of the double cubic group and the Γ_8 is the four-dimensional representation. Which of these five energy levels, corresponding to the different irreducible representations, lies lowest can be calculated in terms of the crystal-field Hamiltonian having a definite total angular momentum *J*,

$$H=B_4(O_4^0+5O_4^4)+B_6(O_6^0-21O_6^4), \tag{3}$$

where O_n^m are the equivalent crystal-field operators expressed as components of J.[23] The coefficients B_4 and B_6determine the scale of the crystal-field splitting. In order to solve the Hamiltonian in Eq. (3) Lea, Leask, and Wolf[24] defined two parameters x and W such that

$$B_4F(4)=Wx, \quad \text{and} \quad B_6F(6)=W(1-|x|), \tag{4}$$

where W is an energy scale factor and $F(4)$ and $F(6)$ are numerical factors chosen to keep the fourth- and sixth-order matrix elements in the same numerical range; for J

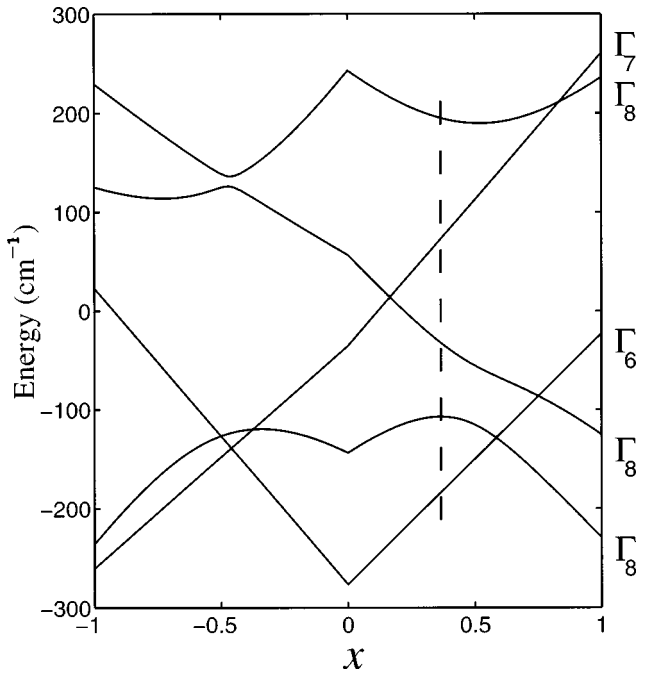

FIG. 11. Crystal-field energy splitting for $J=\frac{15}{2}$ in a cubic crystal field in T_d symmetry with $W=0.8635\ \mathrm{cm}^{-1}$. x is the crystal-field mixing parameter as defined by Eq. (4). The dashed line corresponds to $x=0.35$.

$=15/2, F(4)=60$, and $F(6)=13860$.[24] x is the crystal-field mixing term and is expressed in terms of the ratio of B_4 to B_6 and runs from -1 to $+1$. The eigenvectors of the Hamiltonian are a combination of the fourth- and sixth-order crystal-field potentials. The eigenvalues can be related to the crystal-field energy levels deduced from the observed PL spectrum by the scale parameter W. Negative values of x correspond to tetrahedral coordination, whereas positive values of x occur for octahedral coordination. The crystal-field energy level diagram for Er^{3+} is shown in Fig. 11. With labeling appropriate to T_d symmetry, the Γ_7 representation lies lowest for $-1<x<-0.46$, the Γ_6 representation for $-0.46<x<0.58$, and the Γ_8 representation for $x>0.58$. The Γ_6 and Γ_7 representations can be regarded as doublets and application of the Zeeman magnetic field lifts the Kramers degeneracy and EPR can occur between the two time reversed states. Since the Zeeman splitting is small compared to the differences between the crystal-field energy levels, the Zeeman interaction can be regarded as a perturbation to the crystal-field eigenstates. Using the crystal-field eigenstates given elsewhere[25] the g values associated with transitions within the Γ_6 and Γ_7 states in cubic symmetry are 6.80 and 6.00, respectively. Paramagnetic resonance can also be observed from a Γ_8 quartet. However, the Hamiltonian associated with a Γ_8 state in cubic symmetry (or the two zero-field split levels derived from a Γ_8 state if the symmetry is less than cubic) contains in addition to those terms found in Eq. (1), third-order spin terms of the form S_i^3, where $i=x,y,z$.[25] These third-order terms are significant when the spin-orbit interaction is strong and the absence of these terms in Eq. (1) indicates that the centers do not involve Γ_8 symmetry.

If the overall crystal field has less than cubic symmetry, the principal components of the g tensor can be related to the g value predicted for cubic symmetry g_c by[26–28]

$$g_c=g_{\mathrm{av}}\equiv\tfrac{1}{3}(g_1+g_2+g_3). \tag{5}$$

This approach is only valid if the lower symmetry crystal field is small when compared to cubic crystal field.[26,27] This analysis is also only valid where the g value in cubic symmetry is independent of the strength of the crystal field, which in this case is for the Γ_6 or Γ_7 states. This approach has been used successfully in the interpretation of rare-earth EPR spectra.[26–28] Small differences (<0.04) between g_c and g_{av} are usually explained in terms of interactions with higher-lying energy levels or the effects of covalency.[28] If the difference between the value of g_c and g_{av} is large (>0.1),[28] the assumption that the low symmetry components of the crystal field are small compared to when the cubic crystal field breaks down.

A. Effects of different O concentrations on EPR and PL spectra

It is apparent from Figs. 1 and 2 that in order to observe sharp EPR lines for an Er concentration of 10^{19} Er/cm^3 it is necessary to have in excess of 3×10^{19} O/cm^3. At O concentrations at or below this value, only broad resonances are observed. In the case of sample Er1 (no implanted O present), the single broad isotropic resonance may be due to the formation of Er silicide precipitates. Large clusters of Er silicide are known to form if the Er concentration exceeds 10^{16}/cm^3 (the approximately solubility limit of Er in Si).[7] Although broad resonances are also observed in sample O1 (3×10^{19} O/cm^3),the observed anisotropy of the resonances indicates that the environment around the Er atom has changed due to the inclusion of O. Whilst no sharp EPR lines are observed from this sample it is possible to fit the four observed PL lines to an Er^{3+} center having predominantly cubic symmetry using the crystal-field Hamiltonian given in Eq. (3). The best fit to the experimental data was obtained for $x=0.3544$ and $=0.8635\ \mathrm{cm}^{-1}$ with an rms error in the fit of less than 1.7 cm^{-1}. The position of the fifth energy level consistent with cubic symmetry is predicted to be 372.8 cm^{-1} above the ground state. A transition from the lowest $J=13/2$ energy level to this fifth energy level would appear as a PL line centered at 1.6310 μm. This wavelength lies in a region where the sensitivity of the Ge detector is very low and therefore cannot be detected in the present experiment. A positive sign of x indicates that Er is incorporated in a T_d interstitial site with four nearest neighbors and six next-nearest neighbors lying close by. It is interesting to note that the value of x and W obtained in our analysis are almost identical to those obtained by Przybylinska *et al.*[18] in their study of Er-implanted Si and is consistent with the energy level calculation that found the tetrahedral interstitial site to be the most stable for Er to occupy in Si.[29] These calculations were performed for Er incorporated into pure silicon with no extra impurity present. Furthermore Wahl *et al.*[30] have recently experimentally demonstrated, by the emission channeling technique, that Er is in a tetrahedral interstitial site in float zone Si. A value of $x=0.35$ would imply that the crystal-field ground state has a Γ_6 representation and a single sharp isotropic EPR spectrum with a g value of 6.8 would be predicted. As mentioned previously no sharp EPR line is observed from sample O1 and therefore such cubic Er^{3+} cen-

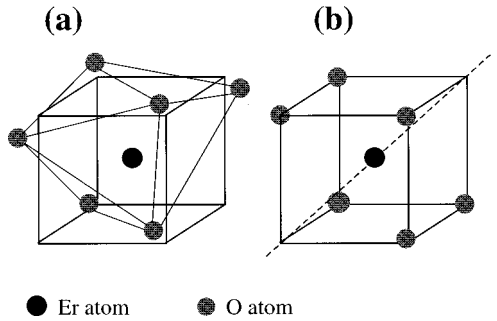

FIG. 12. The arrangement of the O atoms in the local structure around Er in Er_2O_3 giving rise to (a) monoclinic symmetry and (b) trigonal symmetry. Both structures are similar to the cubic fluorite structure but with $\frac{1}{4}$ of the O atoms removed. In the case of the monoclinic centers the missing O atoms are taken from a face diagonal and in the trigonal center the missing atoms are taken from a body diagonal.

ters cannot be the predominantly EPR active centers. However, we can conclude from the anisotropy of the observed EPR spectrum of sample O1 that the EPR active center(s) present has (have) some definite orientation and the fact that it is only seen after coimplantation with 3×10^{19} O/cm^{3}strongly suggests that the center(s) involves oxygen. The broadness of the lines suggests that the associated g values have a range of values that may arise from a range of different local environments due to the presence of different Er-O-Si and/or Er-O complexes.

At the higher O concentrations of 10^{20}/cm^3 in samples O2 and O4 the dramatic appearance of a much narrower line EPR spectrum implies that much more well-defined EPR centers have formed. Despite the absence of any hyperfine lines as a positive signature of Er, the high degree of anisotropy is indicative of a paramagnetic center where the orbital angular momentum is not appreciably quenched, such as a rare earth ion. Furthermore the similarity of the principal g values for centers OEr-1, OEr-1′, and OEr-3 to those reported[26–28] for other Er^{3+} centers strongly suggest that these centers are Er-related centers. In addition the idea that the centers, and also centers OEr-2, OEr-2′, and OEr-4, involve Er^{3+}, rather than the non-Kramers ion Er^{2+}, is further confirmed by the fact that they were fitted by the spin Hamiltonian in Eq. (1), which is only appropriate for the Kramers Er^{3+} ion.[17] For three reasons we are therefore confident that centers observed here directly involve Er^{3+}. The fact that sharp line EPR spectra are only observed in the presence of a high concentration of O indicates that well-defined Er^{3+}-O complexes are being formed. Since the average g value for center OEr-1 is 6.28 and is sufficiently removed from the g value predicted for cubic symmetry for the Γ_6 or Γ_7 state, the crystal field around the Er atom may have a strong low-symmetry component. Such a low-symmetry crystal field can be found in the rare-earth oxides. Er_2O_3 occurs in two forms each with Er^{3+} surrounded by six O atoms: a monoclinic C_2 center and a trigonal C_{3i} center as shown in Figs. 12(a) and 12(b).[31,32] EPR measurements of Er^{3+} in Y_2O_3, which possesses the same local crystal structure as Er_2O_3, reveals the presence of Er^{3+} in both the monoclinic and trigonal sites.[33] In the case of the monoclinic site the principal g values are $g_z=12.314, g_x=1.645$, and $g_y=4.892$. Not only are the magnitudes of these principal g values similar to those observed for center OEr-1 but also the average g value as defined by Eq. (6) is 6.28, identical to that obtained for center OEr-1. We thus suggest that center OEr-1 (and OEr-1) consists of an Er^{3+} ion surrounded by six O atoms in a configuration similar to the monoclinic center found in Er_2O_3. The average g value of the dominant trigonal center OEr-2′ is 2.39 and since it is well removed from the average g value predicted for a Γ_6 or Γ_7 state, the center OEr-2′ could not result from either one of these states. It has further been shown that this center could not arise from a trigonally split Γ_8 state or from an excited state.[34] Furthermore, the fact that this average g value is sufficiently different from the average g value of the trigonal center observed in Y_2O_3:Er^{3+}(6.27) suggests that center OEr-2′ (and OEr-2) is very different from the trigonal center found in Y_2O_3:Er. However, we believe that this center is another well-defined Er-O complex. The remaining centers are also well defined Er-O and/or Er-O-Si complexes though the exact nature of the centers is unclear.

Unlike the EPR spectra, the PL spectrum from sample O2 given in Fig. 9 is similar to the PL spectrum from sample O1. The four PL lines observed in sample O1 are also present in sample O2 though reduced in intensity. In addition other PL lines, not associated with the cubic center are also observed. From this we conclude that the optically active cubic Er^{3+} center is also present in sample O2 but that the dominant centers responsible for the PL and EPR signals are different.

B. Effects of different anneal treatments on the O codoped samples

We now consider the results for samples O2, O3, O4, and O5, which have the same impurity concentrations (10^{19} Er/cm^3 and 10^{20} O/cm^3) but have been subjected to different postimplantation anneal treatments. After implantation the first 2 μm of Si are amorphous and this region is separated by the amorphous-crystalline (a-c) interface from the underlying crystalline substrate. Recrystallization of the amorphous region will occur once the annealing temperature exceeds the crystallization temperature in Si ($\sim$550 °C).[12] Sample O3 only received thermal treatment *A* and the absence of an EPR signal can be explained in terms of little or no SPE regrowth occurring in this sample. EXAFS measurements on this sample have shown that the six nearest neighbors of Er are all Si and that the local environment is $ErSi_2$ like.[16] At a temperature of 620 °C efficient SPE regrowth is occurring and annealing for 3 h (treatment *B*) is sufficient for the *a-c* Si interface to traverse the implanted region. In the absence of O, Polman *et al.*[12] have shown that recrystallization produces a redistribution of Er atoms through the migration of the Er ahead of the *a-c* interface. This will ultimately lead to the formation of clusters of Er and Si atoms and to the formation of Er silicide precipitates. We suggest that this explains the broad resonance observed from sample Er1. However, when O is coimplanted this redistribution of the Er atoms is inhibited.[4] We have already seen that for low O concentrations (3×10^{10}/cm^3), Er-Si-O complexes form while at high O concentrations (10^{20}/cm^3) Er-Si-O or Er-O complexes are likely to form. Recent EXAFS measurements

made on these samples have also indicated that a strong interaction between Er and O occurs leading to the formation of an O-rich first shell.[16] The EXAFS measurements made on sample O4 reveal that after the regrowth process the first coordination shell around Er is composed of 3 ± 2 Si and 4.4 ± 0.6 O atoms. This gives scope for a variety of Er-Si-O and Er-O complexes and may explain our observation of the large number of EPR centers observed in sample O4. The high temperature anneal at 900 °C for 30 s (sample O2) helps to reduce the spread of different types of Er-O complexes with the result that the intensities of centers OEr-1 and OEr-2 are larger in sample O2 than in sample O4. Furthermore centers OEr-3 and OEr-4, which are easily detected in sample O4, are undetectable from sample O2. Indeed the EXAFS measurements made on sample O2 were best fitted by assuming the presence of an average of 5.1 ± 0.5 O atoms, at an average bond length of 0.227 nm similar to the bond lengths observed in Er_2O_3. However, the absence of any EPR signal from a sample (O5) that has been annealed at 900 °C for 30 min indicates that the Er-O complexes observed in EPR are not thermally stable for such an anneal treatment. Comparing the PL spectra from samples O2 (treatment *C*) and O4 (treatment *B*) shown in Fig. 9 reveals that the additional anneal of 900 °C for 30 s slightly increases the PL intensity though other lines from other optically active centers are also present. This demonstrates the importance of the post implantation annealing conditions in determining the number and type of Er-O complexes. We believe that the principle function of the O atoms is to increase the effective solid solubility of Er in crystalline Si by forming Er-O complexes and that the optically active and EPR active centers may be different.

C. Effects of codoping with F

The principal *g* values obtained for center FEr-1 are given in Table II. Comparing the two sets of principal *g* values for center FEr-1 and OEr-1 a number of similarities are apparent. First, both angular dependencies of the spectra can be fitted to a single monoclinic spin $\frac{1}{2}$ center. Furthermore, the average of the *g* tensor, which can be used as a measure of the strength of the low-symmetry crystal field, is 6.31, similar to that found in OEr-1. Since this value is significantly removed from that calculated for a system with predominantly cubic symmetry, it would indicate that the low-symmetry crystal field around the Er atom may be strong. Since a strong low-symmetry crystal field was observed to occur in O implanted Si:Er and attributed to the formation of low-symmetry oxide complexes, a similar explanation may be used in the case of F implantation. An examination of the rare-earth fluorides indicates that two possible forms exist: an eight-coordinated complex with a structure similar to YF_3 in the form of a distorted tricapped trigonal prism[35] and an 11-coordinated distorted tricapped trigonal prism having the same structure as the mineral tysonite.[36] Under the growth conditions for sample F1, only the YF_3 structure is likely to occur; however, to our knowledge, no EPR measurements have been performed on either material. We believe that Er-F complexes are also formed but the exact structure has yet to be determined. Coimplantation with F should have the added benefit of being able to examine the hyperfine structure from the 100% abundant F^{19} isotope ($I=1/2$); however, if Er is in a structure similar to one of the erbium fluorides then the Er-F distance is approximately 0.33 nm.[37] The interaction between Er and F may then be treated in a similar manner to the coupling between two point dipoles.[36] The magnetic field produced by the nuclear magnetic moment of the F atoms is[37]

$$B=\frac{\mu_0}{4\pi}\frac{\mu}{r^3}, \tag{6}$$

where $\mu=g_N\mu_N I$ and g_N is 5.256.[38] The magnetic field experienced by the Er atom, taken to be at the Er-F distance of 0.33 nm, is only 37 μT. Thus even if the Er atom were surrounded by say eight identical F atoms, the total spacing between the outermost F hyperfine lines would only be 296 μT. Since the peak-to-peak width of lines 2 and 3 in Fig. 10 is 1.20 and 1.45 mT, respectively, it is not unreasonable that no F hyperfine interaction is revealed. It is interesting to note that unlike the case of coimplantation with O, coimplantation of 10^{20} F/cm^3 leads only to one well-defined Er-F complex. The PL spectrum from this sample[13] does not reveal any sharp lines and therefore may be unrelated to the FEr-1 center.

V. CONCLUSIONS

Electron paramagnetic resonance spectroscopy has revealed the presence of several Er-impurity complexes, the type and number of which have been shown to depend on the nature and concentration of the implanted impurity and on the annealing conditions. For an Er concentration of 10^{19}/cm^3, the observed EPR spectra depend critically on the O concentration. In the absence of O, Er is surrounded by a cage of Si atoms and for low O concentrations this cage consists of a mixture of O and Si atoms. At high O concentrations the cage is dominated by O atoms and the two dominant centers have monoclinic symmetry and trigonal symmetry. No Er^{3+} in cubic sites was detected by EPR. The EPR active and PL active centers have been shown to be different and we believe that the principal function of the impurity atoms is to prevent precipitation by forming Er-O or Er-F complexes, which leads to an increase in the effective solid solubility of Er in crystalline Si.

ACKNOWLEDGMENTS

The work in Catania has been supported in part by the EU Project SCOOP and by ''Progetto Finalizzato'' MADESS II of CNR.

*Present address: Department of Electronic and Electrical Engineering, University of Surrey, Guildford, GU2 5XH, United Kingdom. Electronic address: D.Carey@ee.surrey.ac.uk

[1] See, for example, *Rare Earth Doped Semiconductors*, edited by G. S. Pomrenke, P. B. Klein, and D. W. Langer, MRS Symposia Proceedings No. 301 (Materials Research Society, Pittsburgh, 1993).

[2] See, for example, *Rare Earth Doped Semiconductors II*, edited by S. Coffa, A. Polman, and R. N. Schwartz, MRS Symposia Proceedings No. 422 (Materials Research Society, Pittsburgh, 1996).

[3] J. Michel, J. L. Benton, R. F. Ferrante, D. C. Jacobson, D. J. Eaglesham, E. A. Fitzgerald, Y. H. Xie, J. M. Poate, and L. C. Kimerling, J. Appl. Phys. **70**, 2672 (1991).

[4] S. Coffa, F. Priolo, G. Franzò, V. Bellani, A. Carnera, and C. Spinella, Phys. Rev. B **48**, 11 782 (1993).

[5] G. Franzò, F. Priolo, S. Coffa, A. Polman, and A. Carnera, Appl. Phys. Lett. **64**, 2235 (1994); G. Franzò, S. Coffa, F. Priolo, and C. Spinella, J. Appl. Phys. **81**, 2784 (1997).

[6] S. Coffa, G. Franzò, F. Priolo, A. Polman, and R. Serna, Phys. Rev. B **49**, 16 313 (1994).

[7] G. Franzò, F. Priolo, S. Coffa, A. Polman, and A. Carnera, Nucl. Instrum. Methods Phys. Res. B **96**, 374 (1995).

[8] F. Y. G. Ren, J. Michel, Q. Sun-Paduano, B. Zheng, H. Kitagawa, D. C. Jacobson, J. M. Poate, and L. C. Kimerling, in *Rare Earth Doped Semiconductors*, edited by G. S. Pomrenke, P. K. Klein, and D. W. Larger, MRS Symposia Proceedings No. 301 (Materials Research Society, Pittsburgh, 1993), p. 87.

[9] R. Serna, M. Lohmeier, P. M. Zagwijn, E. Vlieg, and A. Polman, Appl. Phys. Lett. **66**, 1385 (1995).

[10] J. Stimmer, A. Reittinger, J. F. Nutzel, G. Abstreiter, H. Holzbrecher, and Ch. Buchal, Appl. Phys. Lett. **68**, 3290 (1996).

[11] M. Morse, B. Zheng, J. Palm, X. Duan, and L. C. Kimerling, in *Rare Earth Doped Semiconductors II*, edited by S. Coffa, A. Polman, and R. N. Schwartz, MRS Symposia Proceedings No. 422 (Materials Research Society, Pittsburgh, 1996), p. 41.

[12] A. Polman, J. S. Custer, E. Snoeks, and G. N. van der Hoven, Appl. Phys. Lett. **62**, 507 (1993).

[13] F. Priolo, G. Franzò, S. Coffa, A. Polman, S. Libertino, R. Barklie, and D. Carey, J. Appl. Phys. **78**, 3874 (1995).

[14] S. Libertino, S. Coffa, G. Franzò, and F. Priolo, J. Appl. Phys. **78**, 3867 (1995).

[15] D. L. Adler, D. C. Jacobson, D. J. Eaglesham, M. A. Marcus, J. L. Benton, J. M. Poate, and P. H. Citrin, Appl. Phys. Lett. **61**, 2181 (1992).

[16] A. Terrasi, G. Franzò, S. Coffa, F. Priolo, F. D'Acapito, and S. Mobilio, Appl. Phys. Lett. **70**, 1712 (1997).

[17] A. Abragam and B. Bleaney, *Electron Paramagnetic Resonance of Transition Ions* (Oxford University Press, Oxford, 1970), p. 213.

[18] H. Przybylinska, J. Enzenhofer, G. Hendorfer, M. Schoisswohl, L. Palmetshofer, and W. Jantsch, Mater. Sci. Forum **143–147**, 715 (1994).

[19] J. D. Carey, J. F. Donegan, R. C. Barklie, F. Priolo, G. Franzò, and S. Coffa, Appl. Phys. Lett. **69**, 3854 (1996).

[20] W. Low and R. S. Rubins, Phys. Rev. **131**, 1527 (1963).

[21] B. G. Wybourne, *Spectroscopic Properties of Rare Earths* (Interscience, New York, 1965), p. 28.

[22] A. Abragam and B. Bleaney, *Electron Paramagnetic Resonance of Transition Ions* (Oxford University Press, Oxford, 1970), p. 858.

[23] M. T. Hutchings, in *Solid State Physics 14*, edited by F. Seitz and D. Turnball (Academic, New York, 1964), p. 227.

[24] K. R. Lea, M. J. M. Leask, and W. P. Wolf, J. Phys. Chem. Solids **23**, 1381 (1962).

[25] A. Kingsley and M. Aven, Phys. Rev. **155**, 255 (1967).

[26] J. Dziesiaty, St. Muller, R. Boyn, Th. Buhrow, A. Klimakow, and J. Kreissl, J. Phys.: Condens. Matter **7**, 4271 (1995).

[27] U. Ranon and W. Low, Phys. Rev. **132**, 1609 (1963).

[28] R. K. Watts and W. C. Holton, Phys. Rev. **173**, 417 (1968).

[29] M. Needles, M. Schluter, and M. Lannoo, Phys. Rev. B **47**, 15 533 (1993).

[30] U. Wahl, A. Vantomme, G. Langouche, J. Marques, and J. G. Correia, Phys. Rev. Lett. **79**, 2069 (1997).

[31] G. Brauer, in *Progress in the Science and Technology of the Rare Earths*, Vol. 1, edited by L. Eyring (Pergamon, New York, 1964), p. 155.

[32] R. M. Moon, W. C. Koehler, H. R. Child, and L. J. Raubenheimer, Phys. Rev. **176**, 722 (1968).

[33] G. Schafer and S. Scheller, Phys. Kondens. Mater. **5**, 48 (1966).

[34] J. D. Carey, Ph.D. thesis, University of Dublin, Trinity College, 1997.

[35] A. Zalkin and D. H. Templeton, J. Am. Chem. Soc. **75**, 2453 (1953).

[36] N. N. Greenwood and A. Earnshaw, *Chemistry of the Elements* (Butterworth and Heinmann, Oxford, 1984), p. 1074.

[37] A. Abragam and B. Bleaney, *Electron Paramagnetic Resonance Ions* (Oxford University Press, Oxford, 1970), p. 690.

[38] G. W. C. Kaye and T. H. Laby, *Tables of Physical and Chemical Constants and Some Mathematical Functions*, 14th ed. (Longman, London, 1973), p. 201.